PHYSICAL REVIEW B, VOLUME 65, 174105

Quantitative structure factor and density measurements of high-pressure fluids in diamond anvil cells by x-ray diffraction: Argon and water

Jon H. Eggert,[1,2] Gunnar Weck,[1] Paul Loubeyre,[1] and Mohamed Mezouar[3]
[1]*DIF/DPTA/SPMC, CEA, 91680 Bruyres-le-Châtel, France*
[2]*Lawrence Livermore National Laboratory, P.O. Box 808, Livermore, California 94550*
[3]*European Synchrotron Radiation Facility, BP 220, 38043 Grenoble, France*

(Received 14 September 2001; published 22 April 2002)

We report quantitatively accurate high-pressure, structure-factor measurements of fluids in diamond anvil cells (DAC's) using x-ray diffraction. In the analysis of our diffraction data, we found it possible (and necessary) to determine the density directly. Thus, we also present a diffraction-based determination of the equation of state for fluid water. The analysis of these measurements is difficult since the diamond anvils are many times as thick as the sample and excessive care must be taken in the background subtraction. Due to the novel nature of the experiment and the complexity of the analysis, this paper is concerned primarily with a careful exposition of our analytical methods. Our analysis is applicable to both atomic and molecular fluids and glasses, and we present results for the structure factor and density of two relatively low-*Z* liquids: argon and water. In order to validate our methods we present an extensive comparison of our measurements on water at $P \simeq 0$ in a DAC to recent state-of-the-art x-ray and neutron diffraction experiments and to first-principles simulations at ambient conditions.

DOI: 10.1103/PhysRevB.65.174105 PACS number(s): 62.50.+p, 61.20.−p, 61.10.−i

I. INTRODUCTION

The study of the structure of liquids at high pressure and temperature has been a long-standing goal in high-pressure research. With the maturation of third-generation synchrotron sources this goal is now attainable.[1–3] As with many new techniques applied at high pressure, the extraction of structural information at high pressure has led immediately to novel and interesting physics, as demonstrated by the recent observation of a first-order liquid-liquid phase transition in phosphorus at 1 GPa and 1000 K in a large-volume press.[1]

A major difficulty with liquid diffraction at high pressure is the large background signal generated by the pressure vessel. In large-volume presses this can be overcome using energy-dispersive diffraction and careful spatial filtering of the scattered radiation[1] or using angle-dispersive diffraction and precise Soller slits.[4] Neither approach is possible with the much smaller sample volumes required for diamond-anvil-cell (DAC) studies. Thus, while qualitative estimates of peak positions in the radial distribution function have been obtained in glasses,[6,5] quantitative structural information has never before been obtained in DAC experiments. High-quality structure-factor determinations are critical to successful interpretation of the structure of liquids at extreme conditions, and it was the goal of the present research to obtain such data.

Most of the recent work on the structure of liquids at high pressure and temperature has been done on solids (at ambient conditions) like phosphorous,[1] iron,[2] selenium,[3] or $GeSe_2$.[7] It is our desire to study relatively low-*Z* molecular systems such as argon, H_2O, O_2, and CO_2 because of their high compressibility, complex solid structures, dissociation, and electronic and ionic transitions. These liquids and gases (at ambient conditions) can be easily loaded into a DAC but are very difficult to study in large-volume presses. Unfortunately, the low scattering intensity of low-*Z* materials and the small sample size in DAC experiments make these studies extraordinarily difficult. Even so, we report the measurements and analysis that have allowed us to extract accurate structure factors of both atomic and molecular liquids from DAC experiments. In order to analyze our data we have found it possible and necessary to directly determine the density from the diffraction measurements. Thus, our experiments yield both structural and equation-of-state information. This paper will be aimed primarily at presenting our analysis, with very detailed results given at several pressures for two relatively low-*Z* materials—argon and water—to demonstrate the accuracy of the method.

II. EXPERIMENT

Using standard procedures, we loaded high–purity argon and water samples into specially modified membrane-diamond-anvil cells[8] (MDAC's) with large-angle access ($2\theta_{max} = 36°$) as shown in Fig. 1. The diamond–anvil seats were made of boron to give high x-ray transmission over the full aperture of the DAC's. The pressure was measured using the temperature-corrected hydrostatic ruby pressure scale.[9] While we will only present results for room-temperature experiments, we have performed experiments up to 800 K (Ref. 10) and we will discuss the analytical difficulties presented by high temperatures.

We performed angle-dispersive x-ray diffraction on the ID09 and ID30 beamlines at the European Synchrotron Radiation Facility (ESRF). We used a doubly focused monochromatic beam with wavelength $\lambda = 0.3738$ Å, allowing a maximum momentum transfer of $Q_{max} = 4\pi \sin\theta_{max}/\lambda \sim 100\ \mathrm{nm}^{-1}$. The beam was focused to a diameter between 20 and 80 μm depending on the sample size to avoid any contamination of the spectra by diffraction from the gasket. We used two types of on–line scanning image-plate detec-

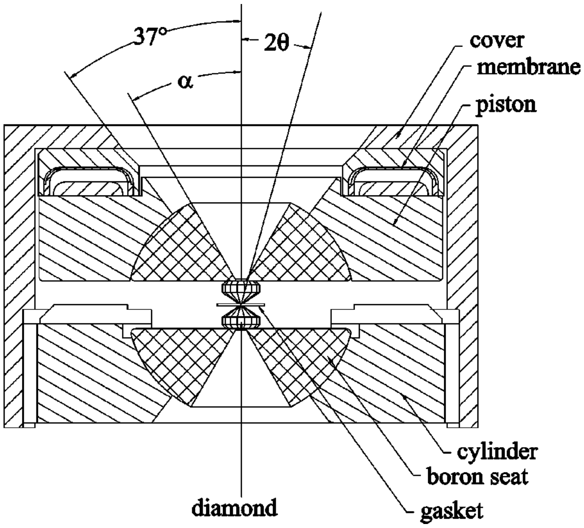

FIG. 1. Diagram of the membrane-diamond-anvil cell (MDAC).

tors: a FASTSCAN (Ref. 11) and a MAR345 (Ref. 12). The sample-detector distance and the detector tilt angles were measured using powder diffraction from a silicon standard. The x-ray beam was 99% horizontally polarized, and all geometric and polarization corrections were made during the angular integration by the program FIT2D.[13,14]

Since temperature diffuse scattering from the diamond anvils varies with temperature, it is necessary to use a background reference spectra at the same temperature as the sample. Thus, we found it useful to develop a way to utilize both empty-cell and solid-sample reference spectra. To obtain empty–cell backgrounds we generally had to disassemble the MDAC and reposition the cell as accurately as possible, while obtaining a solid-sample reference merely involved raising the pressure to above freezing. To eliminate Bragg diffraction from the diamonds we masked the Bragg peaks before performing the angular integrations, being sure to use the same mask for all spectra in an experiment. For the solid-sample backgrounds we eliminated the Bragg peaks from the sample by peak fitting after the angular integration. Typical exposure times were from 1 to 10 min to achieve high exposure over the image plates while avoiding saturation.

III. ANALYSIS

Since the diffuse scattering in a DAC experiment is dominated by background scattering (by one or two orders of magnitude at large Q), the analysis is necessarily different than for most liquid diffraction experiments where background scattering is minimized. Thus we will give a detailed derivation and very general equations applicable to monatomic, molecular, polymeric, and alloy liquids so that our results can be clearly interpreted. While we will refer to a liquid sample, our method can be applied to any amorphous material. The following two sections present a very standard treatment of liquid diffraction in monatomic and polyatomic samples (e.g., Ref. 15), but are included here to define our subsequent notation and to allow proper comparison of our results with other x-ray and neutron diffraction experiments, and with simulations.

A. Monatomic case

The Debye scattering equation[16,15] gives the spherically averaged coherent x-ray scattering from N disordered atoms as

$$I^{coh}(Q)=\sum_{m}^{N}\sum_{n}^{N} f_m(Q)f_n(Q)\frac{\sin Qr_{mn}}{Qr_{mn}}, \tag{1}$$

where $Q=4\pi\sin\theta/\lambda$ is the scattering momentum, $f_m(Q)$ is the atomic form factor for atom m, and r_{mn} is the distance between atoms m and n. We first restrict ourselves to a monatomic liquid of identical atoms and separate the terms with $m=n$ to find

$$I^{coh}(Q)=Nf^2(Q)\left(1+\sum_{n\neq m}\frac{\sin Qr_{mn}}{Qr_{mn}}\right). \tag{2}$$

We define an average atomic density function $\rho(r)$ such that $\rho(r)dV\equiv\langle\rho_m(r_{mn})dV_n\rangle_{\mathcal{S}}$ is the average number of atom centers in the volume element dV at distance r from a central atom, and rewrite the summation as an integral over the x-ray-illuminated sample volume $\mathcal{S}$:

$$I^{coh}(Q)=Nf^2(Q)\left\{1+\int_{\mathcal{S}}\rho(r)\frac{\sin Qr}{Qr}dV\right\}. \tag{3}$$

Adding and subtracting an average atomic density ρ_0 (constant in $\mathcal{S}$, and 0 elsewhere) we find

$$I^{coh}(Q)=Nf^2(Q)\left\{1+\int[\rho(r)-\rho_0]\frac{\sin Qr}{Qr}dV + \int\rho_0\frac{\sin Qr}{Qr}dV\right\}, \tag{4}$$

where the integrals are now over all space. The last term in this equation represents the scattering from a hypothetical object with the shape of the sample and a constant density. This “central scattering,” occurs at such small angles that it is generally blocked along with the direct beam. Thus, we are left with the experimentally observable coherent scattering from N disordered atoms:

$$I^{coh}(Q)=Nf^2(Q)\left\{1+\int_0^\infty[\rho(r)-\rho_0]\frac{\sin Qr}{Qr}4\pi r^2dr\right\}. \tag{5}$$

The structure factor is defined as

$$S(Q)\equiv\frac{I^{coh}(Q)}{Nf^2(Q)}=1+\int_0^\infty[\rho(r)-\rho_0]\frac{\sin Qr}{Qr}4\pi r^2dr. \tag{6}$$

Using the Fourier integral theorem we can transform this equation to find

$$F(r) \equiv 4\pi r[\rho(r)-\rho_0] = \frac{2}{\pi}\int_0^{Q_{max}} Q i(Q)\sin(Qr)\,dQ, \tag{7}$$

where $i(Q)=S(Q)-1$. This expression is exact for $Q_{max}=\infty$, but any experiment must have a finite Q_{max} leading to extraneous peaks and a broadened $\rho(r)$. We shall consider the effects of this finite-cutoff error later.

B. Polyatomic case

For polyatomic liquids, we first define a compositional unit, the choice of which is obvious for stoichiometric compositions and can be fractional for alloys (with appropriate interpretations made for the *intra*molecular summations). Equation (2) then becomes

$$I^{coh}(Q) = N\sum_p f_p^2(Q) + \sum_m \sum_{n\neq m} f_m(Q) f_n(Q)\frac{\sin Qr_{mn}}{Qr_{mn}}, \tag{8}$$

where N is now the total number of compositional units in the sample. We have adopted the convention that p and q index atoms within a compositional unit, while m and n index all atoms in $\mathcal{S}$. As before, we can form an integral equation by defining average atomic density functions $\rho_{p,q}(r)$ such that $\rho_{p,q}(r)dV \equiv \langle \rho_p(r_{p,q})dV_q\rangle_{\mathcal{S}}$ is the average number of atom centers of type q in the volume element dV at a distance r from an atom of type p:

$$I^{coh}(Q) = N\sum_p f_p^2(Q) + N\sum_p \sum_q \int_{\mathcal{S}} f_p(Q) f_q(Q)\rho_{p,q}(r)\frac{\sin Qr}{Qr}dV. \tag{9}$$

We now define several effective parameters in order to reformulate this in terms of an effective molecular density function. We define an effective electronic form factor

$$f_e(Q) \equiv \frac{\sum f_p(Q)}{Z_{tot}}, \tag{10}$$

an effective atomic number

$$K_p(Q) \equiv \frac{f_p(Q)}{f_e(Q)}, \tag{11}$$

and an effective molecular density function

$$\rho_{mol}(Q,r) \equiv \frac{\sum\sum K_p(Q)K_q(Q)\rho_{p,q}(r)}{Z_{tot}^2}, \tag{12}$$

where $Z_{tot}=\Sigma Z_p = \Sigma K_p(Q)$ is the total atomic number of the compositional unit, and we use the analytic tabulation of Hajdu[17] to evaluate the atomic form factors $f_p(Q)$. With these definitions, Eq. (9) becomes

$$I^{coh}(Q) = N f_e^2(Q)\left\{\sum_p K_p^2(Q) + Z_{tot}^2\int_{\mathcal{S}} \rho_{mol}(Q,r)\frac{\sin Qr}{Qr}dV\right\}. \tag{13}$$

Unfortunately, since $\rho_{mol}(Q,r)$ is a function of both Q and r, we cannot directly transform this equation to find the molecular density as we did for Eq. (3) in the atomic case.

Instead, we will adopt a standard approximation that, while detracting from the exactness of the treatment, gives useful results and allows us to proceed.[15] We remove the Q dependence of $K_p(Q)$ by defining an average effective atomic number over the Q range at which we are working:

$$K_p \equiv \langle K_p(Q)\rangle_Q. \tag{14}$$

As an example, for water with $Q_{max}=85\ \mathrm{nm}^{-1}$, K_O and K_H are 9.00 and 0.50, respectively, while for $Q_{max}=95\ \mathrm{nm}^{-1}$ they are 9.08 and 0.46 [note that in the case of *monatomic* molecules such as oxygen, $K_p(Q)$ is *not* a function of Q and the approximation is exact]. The effective molecular density function also loses its Q dependence,

$$\rho_{mol}(r) \equiv \frac{\sum\sum K_p K_q \rho_{p,q}(r)}{Z_{tot}^2}, \tag{15}$$

and Eq. (13) becomes

$$I^{coh}(Q) = N f_e^2(Q)\left\{\sum_p K_p^2 + Z_{tot}^2\int_{\mathcal{S}} \rho_{mol}(r)\frac{\sin Qr}{Qr}dV\right\}, \tag{16}$$

which *can* be Fourier transformed. As in the atomic case, we define an average molecular density ρ_0, ignore the small-angle central scattering and find

$$I^{coh}(Q) = N f_e^2(Q)\left\{\sum_p K_p^2 + Z_{tot}^2 \times \int_0^\infty [\rho_{mol}(r)-\rho_0]\frac{\sin Qr}{Qr}4\pi r^2 dr\right\}. \tag{17}$$

The molecular structure factor is now identified as

$$S_{mol}(Q) = \frac{I^{coh}(Q)}{N Z_{tot}^2 f_e^2(Q)} = S_\infty + \int_0^\infty [\rho_{mol}(r)-\rho_0]\frac{\sin Qr}{Qr}4\pi r^2 dr, \tag{18}$$

where

$$S_\infty \equiv \frac{\sum K_p^2}{Z_{tot}^2}, \tag{19}$$

and we can Fourier transform the equation to find

$$F(r)\equiv 4\pi r[\rho_{mol}(r)-\rho_0]=\frac{2}{\pi}\int_0^{Q_{max}} Qi(Q)\sin(Qr)dQ, \tag{20}$$

where

$$i(Q)=S_{mol}(Q)-S_{\infty}. \tag{21}$$

We can easily identify our effective molecular radial distribution function $g_{mol}(r)$ and note that Eq. (15) allows us to express it as a linear combination of the partial radial distribution functions $g_{p,q}(r)$:

$$g_{mol}(r)\equiv\frac{\rho_{mol}(r)}{\rho_0}=\sum_p\sum_q\frac{K_pK_q}{Z_{tot}^2}g_{p,q}(r). \tag{22}$$

Likewise,

$$S_{mol}(Q)\equiv\sum_p\sum_q\frac{K_pK_q}{Z_{tot}^2}(S_{p,q}(Q)-1)+S_{\infty}, \tag{23}$$

where

$$S_{p,q}(Q)\equiv 1+\rho_0\int_0^{\infty}(g_{p,q}(r)-1)\frac{\sin Qr}{Qr}4\pi r^2dr. \tag{24}$$

These equations enable us to quantitatively compare our results to simulations and to isotropic-substitution neutron scattering experiments. We note that unlike other accurate x-ray diffraction analysis at ambient pressure which rely on neutron scattering determinations of $g_{p,q}(r)$ in their analysis,[18] ours is completely self-contained.

Our definition of $f_e(Q)$ ignores the effects of charge transfer and covalent bonding. Although we could force charge transfer by tweaking the K_p's, at high pressures we generally have no criteria (such as dipole moment data) for doing so, and we still would be left with the spherical charge approximation.[18] However, as will be discussed below, we used a self-consistent procedure to "optimize" $f_e(Q)$ which compensates somewhat for these and other effects.

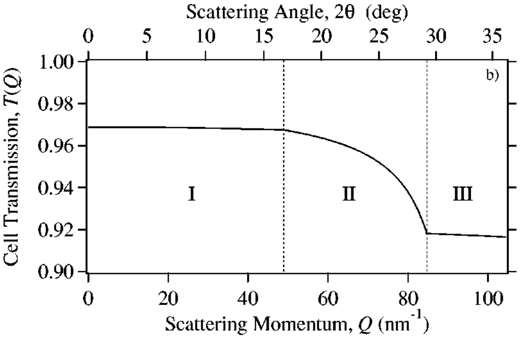

FIG. 2. The calculated transmission function $T(Q)$ for the MDAC shown in Fig. 1 with a diamond anvil thickness of 2.5 mm and $\alpha=30°$. Note that there are three distinct regions: I, the sample diffraction is only absorbed by the diamond anvil; II, the sample diffraction is absorbed by the diamond anvil and the angled part of the boron seat (this is not a step function because the cell is designed to optimize the *visible* optical access to the sample, taking into account the refractive index of the diamond anvil); III, the sample diffraction is absorbed by the diamond anvil and the boron seat.

C. Data treatment

We can separate the experimentally measured scattered intensity $I^{meas}(Q)$ into sample and background contributions modified by several factors:

$$I^{meas}(Q)=T(Q)I^{samp}(Q)+sI^{bkgd}(Q), \tag{25}$$

where $T(Q)$ and s are DAC transmission and scale factors, respectively, $I^{bkgd}(Q)$ is the empty-cell background scattering, and

$$I^{samp}(Q)=\frac{1}{N\alpha}\left[I^{coh}(Q)+N\sum_p I_p^{incoh}(Q)\right] \tag{26}$$

is the total scattering from the sample, where α is the normalization factor to put the signal into atomic units and $I_p^{incoh}(Q)$ is the incoherent (Compton) scattering from atoms of type p in the sample computed using the analytic atomic formulas given by Hajdu.[17] Thus, the experimental determination of $I^{coh}(Q)$ appearing in Eq. (17) is given by

$$I^{coh}(Q)=N\left[\alpha I^{samp}(Q)-\sum_p I_p^{incoh}(Q)\right] \tag{27}$$

and

$$I^{samp}(Q)=\frac{I^{meas}(Q)-sI^{bkgd}(Q)}{T(Q)}. \tag{28}$$

$I^{meas}(Q)$ and $I^{bkgd}(Q)$ are obtained by ϕ integration of the image-plate signal including a polarization correction:

$$I\left(Q=\frac{4\pi\sin(\theta)}{\lambda}\right)=\int_0^{2\pi}\frac{I(2\theta,\phi)}{P(2\theta,\phi)}d\phi, \tag{29}$$

where

$$\begin{aligned}P(2\theta,\phi)=&A_{\parallel}[\sin^2(\phi)+\cos^2(\phi)\cos^2(2\theta)]\\&+A_{\perp}[\cos^2(\phi)+\sin^2(\phi)\cos^2(2\theta)]\end{aligned} \tag{30}$$

is the polarization correction for partially-polarized x-ray radiation[19] where $A_{\parallel}$ and $A_{\perp}$ are the relative x-ray intensities in the primary and perpendicular polarization directions, respectively, θ is the scattering angle, and ϕ is the azimuthal angle from the primary polarization direction. At the ESRF the x rays are 99% polarized and the polarization correction was applied by the image analysis software FIT2D.[13] $T(Q)$ was computed based on our DAC geometry, the absorption coefficients of diamond, and the boron seats (corrected for known impurity concentrations) as shown in Fig. 2. $T(Q)$ was greater than 0.90 for all Q, and reasonable errors in the magnitude and shape of $T(Q)$ had no affect on our results. Since the sample absorption is small for our wavelength and since DAC experiments have very thin samples, we did not correct for sample absorption (however, this could easily be incorporated if found necessary for high-Z materials). Finally, we smoothed $I^{samp}(Q)$ using a cubic-spline smoothing routine[20] which allows the amount of smoothing to vary as a function of Q.

The proper determination of the reference background spectra is probably the most difficult aspect of making and analyzing these measurements. An inherent limitation of a DAC experiment is that scattering from the diamond anvils dominates the signal. We attempted to minimize the background signal by using thick samples (up to 100 μm) and thin diamond anvils (down to 500 μm), but diffuse scattering from the diamonds was still dominant by more than an order of magnitude. Great care must be exercised in collecting the reference spectra with the gasket-hole shape, size, and position identical to that used for the liquid spectra. This is because the metallic gasket serves as an aperture for the diffuse scattering from the first diamond and the shape of $I^{bkgd}(Q)$ is intimately related to this aperture effect. Scattering from the diamonds takes the form of (i) Bragg scattering, which is easily removed by digitally masking the image integration; (ii) Compton scattering, which is assumed to be independent of pressure and temperature; and (iii) temperature diffuse scattering (TDS), which is far more insidious due to its temperature dependence and anisotropy. TDS in a single crystal is concentrated near Bragg peaks giving each peak a broad, temperature-dependent footprint.[15] Since the Bragg and Compton scattering could be treated independently of temperature or pressure, neither offered particular difficulties in obtaining background reference spectra. TDS, on the other hand, necessitates a separate reference spectra for each sample temperature.

Obtaining the empty-cell background $I^{bkgd}(Q)$ after the experiment is often complicated by severe distortion of the sample shape due to sample reactivity and diffusion or catastrophic failure of the diamond anvils at high temperature. These difficulties, coupled with the need for high-temperature reference spectra, led us to develop an alternative method for background subtraction involving the use of a solid-sample background. Since we are often interested in measurements near freezing, it is very easy to collect solid-sample reference spectra. Our ideal experimental procedure entails collecting data along an isothermal pressure scan that crosses the melting curve. This method of background subtraction relies on the fact that the coherent scattering in a crystalline solid is confined to narrow Bragg peaks and the associated TDS. Since the sample Bragg peaks are much sharper than any liquid information, they are easily removed by peak fitting. The incoherent Compton scattering is the same in the crystal or the liquid and has been discussed above. Unfortunately, TDS from the sample is again a major problem due to its complex momentum and temperature dependence. In order to compensate approximately for the TDS we chose the most simple description of TDS possible, assuming that each molecular unit vibrates as a single unit independently of any other atoms. In this case the TDS is isotropic and proportional to a Debye-Waller factor:[15]

$$I^{TDS}(Q)=NZ_{tot}^2 f_e^2(Q)[1-e^{-\langle\mu_s^2\rangle Q^2}], \tag{31}$$

where $\langle\mu_s^2\rangle$ is the mean-square component of the displacement of the molecular units in the scattering direction. The total diffuse scattering arising from Compton scattering and TDS can thus be subtracted from the solid-sample background to give an effective empty-cell background

$$I^{bkgd}(Q)=I_{solid}^{bkgd}(Q)-\frac{NT(Q)}{\alpha'}\left\{\sum_p I_p^{incoh}(Q) - Z_{tot}^2 f_e^2(Q)[1-e^{-\langle\mu_s^2\rangle Q^2}]\right\}. \tag{32}$$

α' is simply a normalization factor to convert from atomic units to experimental intensity. We evaluate both N/α' and $\langle\mu_s^2\rangle$ by making use of the analysis described in the next section applied to several experimental liquid spectra at the same temperature. Details appear in the Appendix.

D. Optimization procedure

We determine the normalization factor α in Eq. (27) using the Krogh-Moe[21] and Norman[22] method, which makes use of the fact that $\lim_{r\to 0}[\rho_{mol}(r)]=0$, $\lim_{r\to 0}[\sin(Qr)]=Qr$, and Eq. (20) to find

$$-2\pi^2\rho_0=\int_0^{Q_{max}} i(Q)Q^2 dQ. \tag{33}$$

Using Eqs. (18), (21), (27), and (33) to solve for α, we find the normalization factor

$$\alpha=Z_{tot}^2\frac{-2\pi^2\rho_0+\int_0^{Q_{max}}[J(Q)+S_\infty]Q^2 dQ}{\int_0^{Q_{max}}\frac{I^{samp}(Q)}{f_e^2(Q)}Q^2 dQ}, \tag{34}$$

where

$$J(Q)\equiv\frac{\sum I_p^{incoh}(Q)}{Z_{tot}^2 f_e^2(Q)}. \tag{35}$$

Unfortunately, the finite value of Q_{max} and the lack of knowledge of ρ_0 for high-pressure liquids make the determination of α somewhat uncertain. Due to the domination of the diamond diffuse background over scattering from the sample, we also need to determine the scale factor s in Eq. (27) with high precision. Accurate direct measurement of the beam intensity is not currently possible on the beamlines we have used, so an alternative method for finding s was needed.

We now present a self-consistent, corrective procedure that addresses all of the above-mentioned problems and even allows us to experimentally determine ρ_0. Following the general outline of a method for minimizing errors in the determination of $g(r)$ pioneered by Kaplow *et al.*,[23] we force the behavior of $F(r)$ at small r (below the first *inter*molecular peak) to match the expected behavior for a given sample. We have identified three areas of systematic uncertainty that we would like to correct: errors in α due to the limited Q

range of the integrals in Eq. (34), errors in $f_e(Q)$ due to molecular-bonding and charge-transfer effects and errors in s due to the impossibility of measuring accurate x-ray fluxes in our experiments. We assume that errors in these variables take the following forms: $\alpha=\alpha_0(1+\Delta\alpha)$, $1/f_e^2(Q)=[1/f_{e0}^2(Q)][1+\Delta f_e(Q)]$, and $s=s_0+\Delta s$, where $\Delta\alpha$ and Δs are constant, and $\Delta f_e(Q)$ varies slowly with Q. Using Eqs. (18), (21), (27), (28), and (34), we can express the error in $i(Q)=i_0(Q)+\Delta i(Q)$ to first order in $\Delta\alpha$, $\Delta f_e(Q)$, and Δs as

$$\Delta i(Q)=\{\Delta\alpha-\delta[\Delta f_e(Q)]+\delta(\Delta s)\}[S_0(Q)+J_0(Q)], \tag{36}$$

where

$$\delta[\Delta f_e(Q)]\equiv\frac{\int\Delta f_e(Q)[S_0(Q)+J_0(Q)(1-Z_{tot}^2)]Q^2dQ}{\int[S_0(Q)+J_0(Q)]Q^2dQ}-\frac{\Delta f_e(Q)S_0(Q)}{S_0(Q)+J_0(Q)} \tag{37}$$

and

$$\delta(\Delta s)\equiv\frac{\Delta s\int\frac{I^{bkgd}(Q)}{T(Q)f_{e0}^2(Q)}Q^2dQ}{\int\frac{I^{samp}(Q)}{f_{e0}^2(Q)}Q^2dQ}-\frac{\Delta sI^{bkgd}(Q)}{T(Q)I^{samp}(Q)}. \tag{38}$$

Kaplow *et al.*[23] considered the special case

$$Q\Delta i(Q)=Q\Delta\alpha S_0(Q)=\Delta\alpha[Qi_0(Q)+QS_\infty], \tag{39}$$

as in Eq. (36) when $\Delta f_e(Q)=0$, $\Delta s=0$, and $J_0(Q)=0$. The first term in Eq. (39) leads to a simple rescaling of $F(r)$ but the second, "ramp" term, leads to oscillations at small r according to

$$\Delta F_{ramp}(r)=\Delta\alpha\frac{2S_\infty}{\pi}\left[\frac{\sin(Q_{max}r)}{r^2}-\frac{Q_{max}\cos(Q_{max}r)}{r}\right]. \tag{40}$$

Figure 3 shows $F(r)$ for argon at 1.1 GPa as well as this function for $\Delta\alpha=1\%$. Obviously, for even a 1% error in α the resulting $g(r)$ is dominated by oscillations due to the error in α. These oscillations are unphysical, dominant at small r, and can be used as an iterative feedback to determine a corrected value for $i(Q)$.

In determining the expected behavior of $F(r)$ at small r we must bear in mind that the effective electronic form factor $f_e(Q)$ does not account for interference effects between atoms in the same molecule. At small r, *intra*molecular peaks should appear in $F(r)$ for molecular samples. Thus, we will use a frozen-molecule formulation and assume that each molecule has a fixed geometry with known interatomic distances. The contribution to $i(Q)$ from the interaction of atoms within the same molecule is then

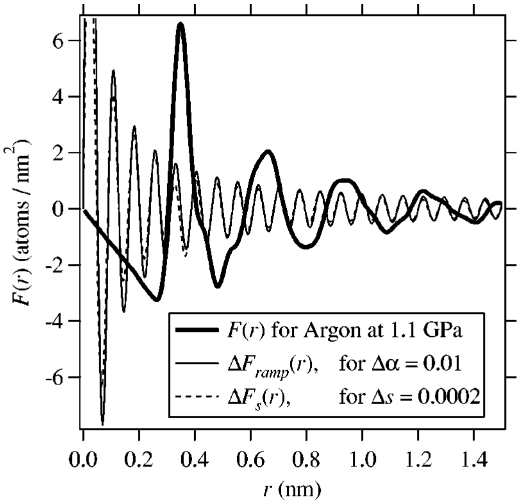

FIG. 3. Effect of errors in α and s compared to $F(r)=4\pi r[\rho(r)-\rho_0]$ for argon at 295 K and 1.1 GPa using $Q_{max}=85\ \text{nm}^{-1}$, $\rho_0=27.2\ \text{atoms/nm}^3$, and $s=1.083\,47$.

$$i_{intra}(Q)=\sum_p\sum_{q\neq p}\frac{K_pK_q}{Z_{tot}^2}\left[\frac{\sin(d_{p,q}Q)}{d_{p,q}Q}\right], \tag{41}$$

where $d_{p,q}$ is the distance between atoms p and q in the molecule. Fourier transforming $Qi_{p,q}(Q)$ we find that the intramolecular contribution to $F(r)$ is

$$F_{intra}(r)=\sum_p\sum_{q\neq p}\frac{K_pK_q}{\pi Z_{tot}^2d_{p,q}}\left\{\frac{\sin[(r-d_{p,q})Q_{max}]}{r-d_{p,q}}-\frac{\sin[(r+d_{p,q})Q_{max}]}{r+d_{p,q}}\right\}. \tag{42}$$

This function has peaks at $r=d_{p,q}$ and several weaker secondary peaks broadened according to the cutoff momentum Q_{max}. In our calculations for molecular liquids we used the gas-phase values for $d_{p,q}$ assumed to be pressure independent.

Note that Eq. (41) is not quite correct for polymeric liquids or framework glasses such as SiO_2 where there is additional *inter*molecular coordination between compositional units. In this case Eq. (41) must be replaced by

$$i_{intra}(Q)=\sum_{P,Q}{}'(2-\delta_{P,Q})n_Pn_{P,Q}\frac{K_PK_Q}{Z_{tot}^2}\left[\frac{\sin(d_{P,Q}Q)}{d_{P,Q}Q}\right], \tag{43}$$

where P and Q denote atom types within the compositional unit, $\delta_{P,Q}$ is the Kronecker delta function, n_P is the number of atoms of type P in the compositional unit, $n_{P,Q}$ is the number of atoms of type Q at distance $d_{P,Q}$ from each atom of type P, and the primed summation denotes the sum over all unique pairs of atom types P and Q.

For r less than the minimum *inter*molecular contribution to $g_{mol}(r)$ $(r<r_{min})$ we evaluate the difference between $F_{(0)}(r)$ calculated from Eq. (20) and its expected behavior,

$$\Delta F_{(0)}(r)=F_{(0)}(r)-[F_{intra}(r)-4\pi r\rho_0], \tag{44}$$

where the parenthetical subscripts denote the iteration number. We now inverse Fourier transform $\Delta F_{(0)}(r)$ to find the term responsible for the small r oscillations [the "ramp" term in Eq. (39)],

$$\Delta\alpha_{(0)}QS_\infty=\int_0^{r_{min}}\Delta F_{(0)}(r)\sin(Qr)dr, \tag{45}$$

and extract an improved estimate of $i(Q)$:

$$\begin{aligned}i_{(1)}(Q)=i_{(0)}(Q)-\Delta\alpha_{(0)}S_{(0)}(Q)=i_{(0)}(Q)\\ -\frac{1}{Q}\left[\frac{i_{(0)}(Q)}{S_\infty}+1\right]\int_0^{r_{min}}\Delta F_{(0)}(r)\sin(Qr)dr.\end{aligned} \tag{46}$$

This leads to an improved value of $F_{(1)}(r)$ with much better behavior at small r.

We now extend this analysis to our situation involving errors in α, as well as in $f_e(Q)$ and s. Note that the first terms in Eqs. (37) and (38) are all independent of Q so that we have, as above, a part that simply scales $F(r)$ and a ramp part that leads to oscillations in $F(r)$ at small r. The second term in Eq. (37), $\Delta f_e(Q)$ is expected to vary slowly in Q and behaves similarly.[23] However, the second term in Eq. (38) is Q dependent and contributes a factor $\Delta F_s(r)$ to the function $F_{(0)}(r)$. Figure 3 plots $\Delta F_s(r)$ for argon at 1.1 GPa assuming $\Delta s=0.0002$. Note the similarity of the effects at small r of errors in α and s. Relaxing the requirement that the Compton scattering correction be negligible $[J_0(Q)=0]$ has little effect on the analysis as noted originally by Kaplow *et al.*[23] Thus, we use the complete expression for the ramp term given by Eq. (36) to obtain an iterative procedure for $F_{(i+1)}(r)$ given an estimate of ρ_0 and s:

$$(1)\quad F_{(i)}(r)=\frac{2}{\pi}\int_0^{Q_{max}}Qi_{(i)}(Q)\sin(Qr)dQ, \tag{47}$$

$$(2)\quad \Delta F_{(i)}(r)=F_{(i)}(r)-[F_{intra}(r)-4\pi r\rho_0], \tag{48}$$

$$\begin{aligned}(3)\quad i_{(i+1)}(Q)=i_{(i)}(Q)-\frac{1}{Q}\left[\frac{i_{(i)}(Q)}{S_\infty+J_0(Q)}+1\right]\\ \times\int_0^{r_{min}}\Delta F_{(i)}(r)\sin(Qr)dr.\end{aligned} \tag{49}$$

The convergence of this process is extremely rapid and two iterations were generally sufficient as shown in Fig. 4.

As Kaplow *et al.*[23] noted, ρ_0 is an independent variable in this analysis with a direct influence on α and $\Delta F_{(n)}(r)$, so that ρ_0 can be extracted by minimizing $\Delta F_{(n)}(r)$. The optimum value for s can similarly be extracted. Thus, we varied the values of ρ_0 and s to minimize $\Delta F_{(n)}(r)$ using a χ^2 figure of merit:

$$\chi^2_{(n)}(\rho_0,s)\equiv\int_0^{r_{min}}[\Delta F_{(n)}(r)]^2dr. \tag{50}$$

From this discussion it is not at all apparent that $\chi^2_{(n)}(\rho_0,s)$ is sufficiently well behaved to allow the determination of either ρ_0 or s, not to mention both of them. However, it turns out that there is a unique, well-defined minimum in $\chi^2_{(n)}$ (for $n\lesssim 4$) and that the variables ρ_0 and s are surprisingly independent. This can be seen in Fig. 5 which shows a contour plot of $\chi^2_{(2)}$ in ρ_0-s space for our argon data at $P=0.6$ GPa and $T=295$ K. The independence of ρ_0 and s is demonstrated by the nearly circular symmetry near the minimum of $\chi^2_{(2)}$ shown in Fig. 5. In fact, we are able to determine the minimum with a high degree of precision. Similar results are found for both atomic and molecular liquids.

It should be noted that the method we have described is very similar to an earlier approach by Gereben and Pusztai[24,25] to determine the density by minimizing χ^2 for a variety of assumed densities in a reverse Monte Carlo (RMC) simulation. Gereben and Pusztai found that the minimum χ^2 corresponded within 3% to the actual density. Our method represents a significant improvement over this RMC method in that the process is so much faster that we can refine both ρ_0 and s in a matter of minutes rather than the hours required for a single RMC simulation.

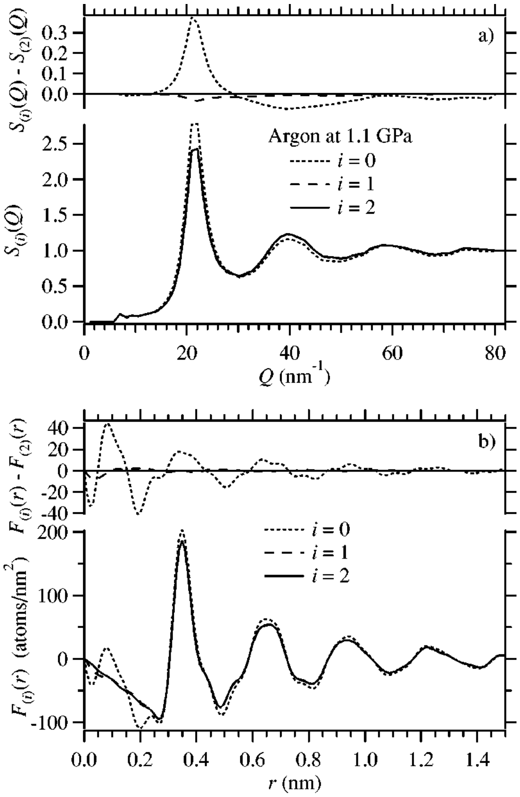

FIG. 4. The structure factor $S_{(i)}(Q)$ and the distribution function Here $F_{(i)}(r)$ for argon at 1.1 GPa as a function of the number of iterations i. Here $F_{(0)}(r)$ shows oscillations at small r reminiscent of those due to errors in α and s, as shown analytically in Fig. 3. Note that these oscillations and any other deviations very nearly converge after only one iteration.

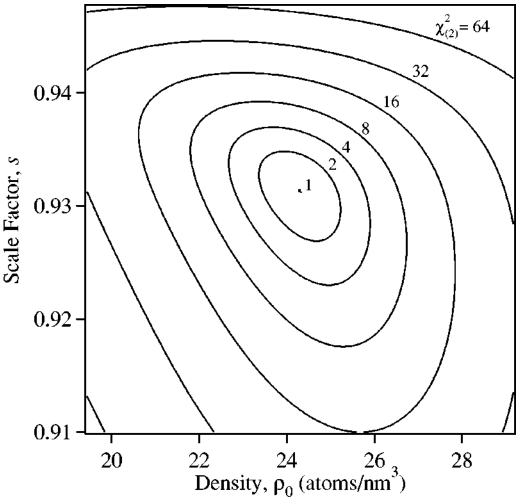

FIG. 5. Contour plot of $\chi^2_{(2)}$ as a function of the atomic density ρ_0 and the scale factor s, for argon at 0.6 GPa. Note that $\chi^2_{(2)}$ has been normalized to 1 at the minimum.

E. Effects of finite Q_{max}

Now we need to address the difficult issue of the effects of the limited Q range over which $S_{mol}(Q)$ can be measured. The weighting of the decreasing experimental signal $I^{coh}(Q)$ by the rapidly increasing factor $1/f_e^2(Q)$ in Eq. (18) makes the high-Q signal increasingly noisy and can lead to dramatic oscillations near the first peak in $F(r)$.[23] We tested the stability of our analysis to varying values of Q_{max} between 60 nm^{-1} and 100 nm^{-1} and found that the optimum values of ρ_0 and s were coupled and varied systematically with Q_{max} as shown in Fig. 6 for water very near ambient pressure.[26]

For our final, reported values of ρ_0 we averaged the determinations from all values of Q_{max} between reasonable limits determined by inspection of the resulting $S_{mol}(Q)$ and $g_{mol}(r)$ spectra (60 nm$^{-1} \leqslant Q_{max} \leqslant 92.5$ nm^{-1}). The reported errors are the standard deviation of these values. Table I shows the excellent agreement between our determination of the density and piston–cylinder measurements for argon.[27]

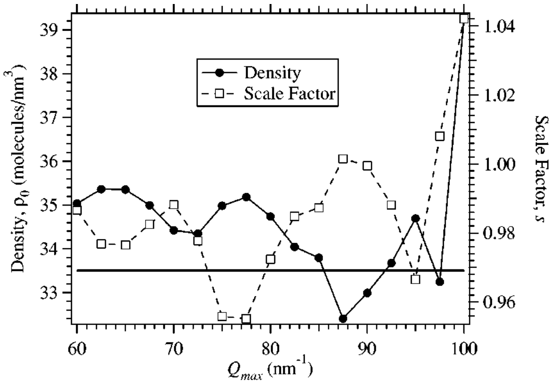

FIG. 6. The optimum density ρ_0 (left axis) and scale factor s (right axis) for water at nearly ambient pressure (Ref. 26) and temperature as a function of Q_{max}. The heavy line is the density of water at ambient conditions.

TABLE I. Experimental densities at room temperature and two pressures for argon determined in this experiment and with a piston-cylinder device.

Pressure (GPa)	Density (atoms/nm^3) This experiment	Density (atoms/nm^3) Ref. 27
0.6	24.2±0.3	24.23
1.1	27.7±0.4	27.74

Figure 7, similarly, shows our determination of the density for liquid water at 295 K plotted against the Saul-Wagner equation of state.[28] The open circles represent an empty-cell reference, while the solid circles represent a solid-sample reference. The agreement between the densities obtained using different references strongly supports the validity of our solid-sample reference method. The excellent agreement between our measurements and the equations of state suggests that our analysis rests on a sound foundation and that it is possible to measure the density of liquids by x-ray diffraction to ~3% accuracy in diamond anvil cells. These density measurements of liquids reported by x-ray diffraction at high pressure open an exciting new possibility of directly measuring the equation of state of liquids.

To generate final values for $S_{mol}(Q)$ and $g_{mol}(r)$ we fixed ρ_0 to its final average value and adjusted s while varying Q_{max} over a range of values for each spectra. The results are shown in Figs. 8 and 9 for water. Note that $S_{mol}(Q)$ is well

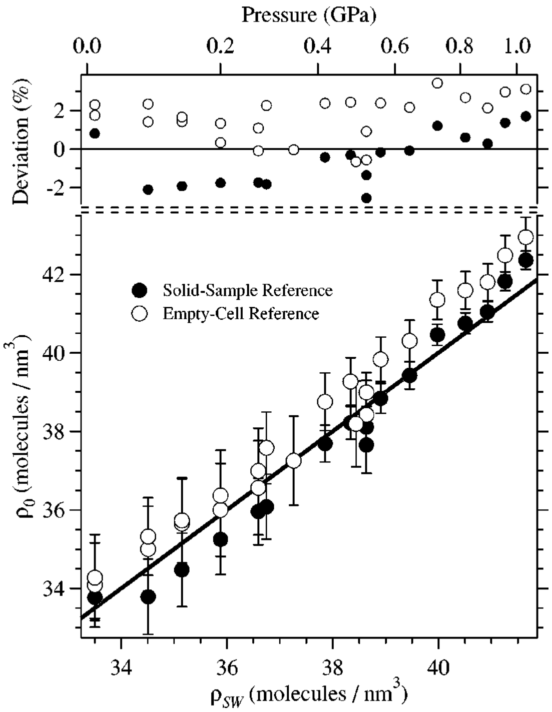

FIG. 7. Our experimental determination of the density ρ_0 of liquid water at 295 K plotted against the Saul-Wagner equation of state density ρ_{SW} (Ref. 28). The pressure scale is shown on the top axis and extends from very nearly 1 bar to above the freezing pressure of 1.0 GPa. The percent-deviation scale shows that our density determination for liquid water has an accuracy of about ±3%.

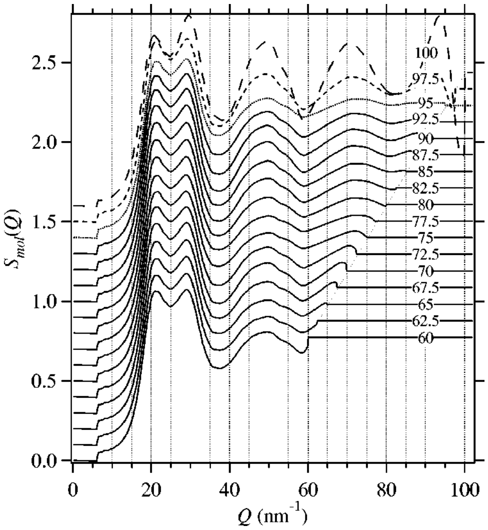

FIG. 8. The molecular structure factor $S_{mol}(Q)$ for nearly ambient pressure (Ref. 26) water determined as a function of Q_{max} using an empty-cell background subtraction and the experimental density, $\rho_0 = 34.3$ molecules/nm^3. Note that the positions of the peaks and valleys, and the shape of the structure factor are very consistent over a wide range of Q_{max} until the obvious distortions due to absorption by the MDAC body begin to appear at $Q_{max} = 95$ nm^{-1}.

behaved over the entire span of Q_{max} while $g_{mol}(r)$ shows oscillations associated with the finite Q cutoff whenever Q_{max} corresponds to a local extremum in $S_{mol}(Q)$. Since $S_{mol}(Q)$ changes only slightly with Q_{max}, we believe that $S_{mol}(Q)$ is relatively unaffected by the Q_{max}-cutoff problem. We believe that our structure factors $S_{mol}(Q)$ obtained in this way are accurate to the point where obvious problems with the $S_{mol}(Q)$ or the $g_{mol}(r)$ spectra ($Q_{max} = 92.5$ nm^{-1}) begin to appear in Figs. 8 and 9. This is not the case for $g_{mol}(r)$ where the Q_{max} cutoff is a serious problem for all Q_{max}. Even so, a simple way to get a reasonable, if not completely accurate, $g_{mol}(r)$ is to simply choose the largest value of Q_{max} that minimizes the unphysical fringes seen in Fig. 9 ($Q_{max} = 85$ nm^{-1}).

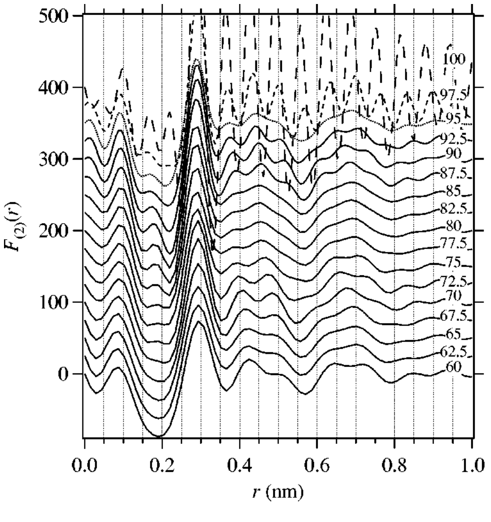

FIG. 9. $F_{(2)}(r)$ for water determined from the structure factors shown in Fig. 8. Note that the position of the first intermolecular peak at $Q \sim 0.29$ nm^{-1}, the next minimum, and the peak width all decrease as Q_{max} increases. In addition, there are strong oscillations in $F_{(2)}(r)$ whenever $S_{mol}(Q_{max})$ is a local extrema. All these effects are due to the finite Q_{max} cutoff in the Fourier transform of $S_{mol}(Q)$. In addition, the very detrimental effect of the MDAC absorption above $Q_{max} = 95$ nm^{-1} is clearly seen. Note that the first peak at $r = 0.095$ nm is due to the *intra*molecular OH distance and was forced by our analysis procedure [Eq. (47)]. The width of this peak is entirely due to the finite Q_{max} according to Eq. (42).

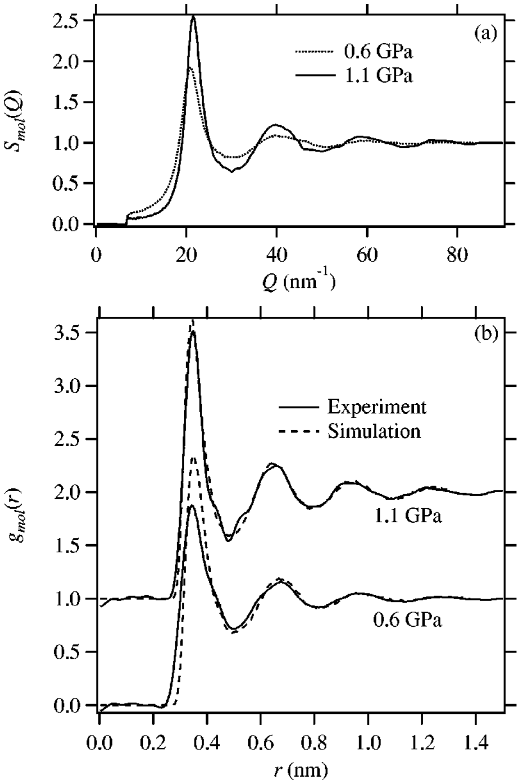

FIG. 10. Results of our experiments on argon at 0.6 and 1.1 GPa. (a) The structure factor $S_{mol}(Q)$. (b) The radial distribution function $g_{mol}(r)$, as well as a molecular dynamics simulation of argon at the experimental densities.

IV. DISCUSSION

Figure 10 shows our experimental structure factors $S(Q)$ and radial distribution functions $g(r)$ for argon at 0.6 and 1.1 GPa. The $g(r)$'s were computed as described above with a "best" Q_{max} of 85 nm^{-1}. As expected, $S(Q)$ and $g(r)$ are more highly structured as the freezing pressure (1.3 GPa) is approached. Also shown are classical molecular dynamics simulations of $g(r)$ using the Aziz pair potential[29] and 512 atoms fixed at the experimental densities. The figure shows very good agreement between the experimental and theoretical peak positions in $g(r)$ and good agreement in the peak heights.

Figure 11(a) shows our $g_{mol}(r)$ for nearly ambient pressure[26] water compared to recent measurements using x-ray[30,18] and neutron[31] diffraction, as well as recent first-principles simulations.[32] In order to compare our results with

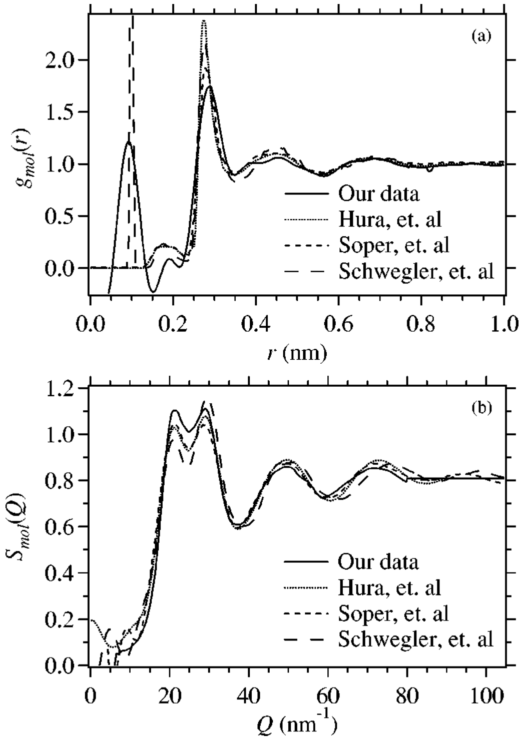

FIG. 11. Results of our experiments on nearly ambient pressure (Ref. 26) water and comparison to other recent experiments by Hura and co-workers (Refs. 30 and 18) and Soper *et al.*, (Ref. 31) and to first-principles simulations (Ref. 32). (a) Comparisons for $g_{mol}(r)$ are to the linear combinations of reported site-site distribution functions according to Eq. (22. (b) Comparisons to $S_{mol}(Q)$ are made to the Fourier transform of the respective $g_{mol}(r)$'s according to Eq. (23). The intensity discrepancy between our $S_{mol}(Q)$ and other experimental determinations is consistent with the existence of a small residual pressure ($P<0.05$ GPa).

previous results we have plotted the linear combinations of reported site-site distribution functions according to Eq. (22). The "best" Q_{max} used to find our $g_{mol}(r)$ was 80 nm^{-1} so that the coefficients are $K_O=8.96$, $K_H=0.52$, and $S_\infty=0.808$. The first peak in our $g_{mol}(r)$ at $r=0.095$ nm is the *intra*molecular-OH peak imposed by our analysis [Eq. (47)] and was not actually measured by us or in any other diffraction experiments, but it was found in the first principles simulations.[32] Since the broadening of this peak in our analysis is entirely due to the Q_{max} cutoff, its width gives a good representation of our experimental resolution in r. The second peak at $r=0.18$ nm is the *inter*molecular–OH peak measured in the neutron experiments and the simulations, but not in the x-ray experiments. We could find no reliable way to introduce this peak in our analysis, and our data are insufficient to measure it. The dominant peak in our $g_{mol}(r)$ at $r\sim0.28$ nm is too broad, too weak, and at too high r compared to the other functions. However, we believe that these inconsistencies can be explained by our finite Q_{max} since the other experiments were analyzed to explicitly eliminate the Q_{max} problem by fitting to a basis set of $g(r)$ functions[18] and by a minimum-noise algorithm.[31] The similarity in peak width of the peaks at $r=0.095$ and 0.28 nm lends support to this view, as does the fact that the integrated intensities of $r^2 g_{mol}(r)$ are all consistent. All the subsequent broader peaks in $g_{mol}(r)$ are in quite good agreement.

To further test our proposition that our determinations of $S_{mol}(Q)$ are accurate, even though our determinations of $g_{mol}(r)$ are hampered by the Q_{max} problem, we compare in Fig. 11(b) our measured structure factor $S_{mol}(Q)$ with those from the same three data sets. To allow a direct comparison, we have performed the inverse Fourier transform [Eq. (23)] of the $g_{mol}(r)$'s shown in Fig. 11(a). We find that our determination of $S_{mol}(Q)$ is in excellent agreement with the other experimental structure factors. All of the peak positions are in good agreement and the peak intensities are very nearly so. The small discrepancy in the relative and total intensities of the primary doublet is entirely consistent with a small (~0.05 GPa) applied pressure[26] according to our and previous high-pressure measurements.[33] There is a distinct difference between the experiments and simulation in the position of the third peak near 72 nm^{-1}, but overall, the agreement in the various $S_{mol}(Q)$'s is very good.

Based upon the comparisons shown in Fig. 11 we feel confident that our determinations of the structure factor $S_{mol}(Q)$ are reliable. In the future, we plan to determine the radial distribution function $g_{mol}(r)$ in a more robust way to eliminate the Q_{max} problem. We are presently examining several approaches including fitting to a basis set of $g(r)$ functions,[18] the minimum-noise algorithm,[31] and a Q-space continuation method.[33]

V. CONCLUSION

We have performed a quantitative measurements of a liquid structure factor in a DAC. In order to account for the temperature-dependent background scattering of the diamond anvil we have developed a solid-sample background subtraction procedure that substantially improves the experimental procedure. Due to the substantial diffuse scattering (Compton and TDS) from the diamond anvil, we were forced to develop a iterative analysis procedure for our measurements. A fortuitous by-product of this analysis is that the bulk density of the fluid can be measured, thereby eliminating a free parameter in all previous studies of high-pressure fluid diffraction. We have demonstrated that the density can be measured to within about 3% in liquid argon and water. This is an accurate and direct method for measuring fluid equations of state in a DAC.

We have performed extensive tests of our analytical method and believe that our resultant structure factors are highly accurate. At this time, we have not obtained radial distribution functions with similar accuracy due to the Q_{max} problem, but many methods have been previously developed and we are confident that these methods applied to our $S_{mol}(Q)$ measurements will yield good results. Ultimately, we hope to employ reverse Monte Carlo algorithms[34] to better determine the structure of our samples. RMC algorithms require quantitatively accurate structure factors that have

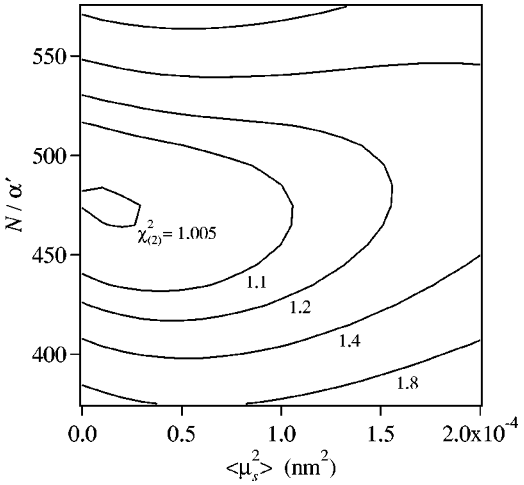

FIG. 12. Contour plot of $\chi^2_{(2)}$ as a function of the diffuse scattering intensity N/α' and the mean-square displacement $\langle\mu_s^2\rangle$, for metastable liquid water at 1.11 GPa and 295 K using a solid ice VI reference spectra taken at 1.08 GPa. Note that $\chi^2_{(2)}$ has been normalized to 1 at the minimum.

previously been impossible to measure at high pressures. It is our hope that our analysis will provide $S_{mol}(Q)$'s at high pressures and temperatures of sufficient accuracy to permit structural studies of novel fluids at very extreme conditions.

ACKNOWLEDGMENTS

We acknowledge the European Synchrotron Radiation Facility for provision of synchrotron radiation facilities, and we would like to thank A. Dewaele, R. Le Toullec, F. Occelli, M. Hanfland, and T. Le Bihan for valuable assistance in these experiments. This work was performed under the auspices of the U. S. Department of Energy by the University of California, Lawrence Livermore National Laboratory under Contract No. W-7405-Eng-48.

APPENDIX

The equation to correct a solid-background reference spectrum for diffuse scattering from the solid is given by Eq. (32) (reproduced below) and includes Compton and temperature diffuse scattering terms:

$$I^{bkgd}(Q)=I^{bkgd}_{solid}(Q)-\frac{NT(Q)}{\alpha'}\left\{\sum_p I^{incoh}_p(Q)\right.$$
$$\left.-Z^2_{tot}f^2_e(Q)[1-e^{-\langle\mu_s^2\rangle Q^2}]\right\}. \qquad \text{(A1)}$$

We treat N/α' and $\langle\mu_s^2\rangle$ as free parameters to be optimized. Figure 12 shows a contour map of the optimized $\chi^2_{(2)}$ versus N/α' and $\langle\mu_s^2\rangle$ for room-temperature liquid water at nearly 0 GPa (Ref. 26) and a solid reference at 1.1 GPa. Note that the contour shape is far from circular, but that there is a well-defined minimum. We found the optimum values of N/α' and $\langle\mu_s^2\rangle$ by minimizing $\chi^2_{(2)}$ for several spectra at or near the same temperature using a single reference spectrum. We then averaged the values of N/α' and $\langle\mu_s^2\rangle$ so obtained to find a corrected background spectrum for use in the analysis. In this way we were able to obtain reliable background spectra from our solid-sample reference spectra for use on liquid spectra at similar temperatures. As an example, Fig. 13 shows the results of such an analysis. The background spectra obtained from solid and empty cells are seen to be very similar and Fig. 14 shows the structure factor obtained using the two backgrounds, respectively. The value of the optimum density obtained from each background was 33.8±0.5 and 34.3±1.1 molecules/nm^3, while the expected value is 33.5 molecules/nm^3.

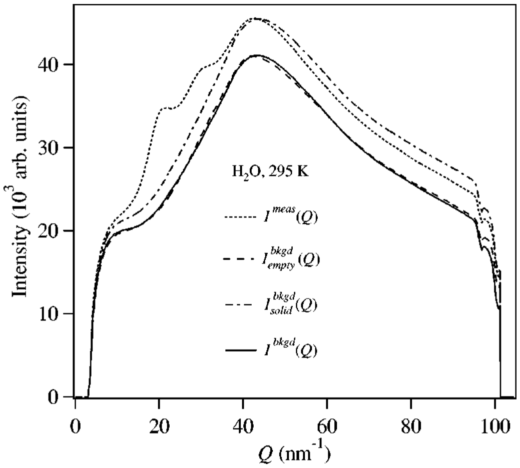

FIG. 13. The measured spectra $I^{meas}(Q)$ for H_2O at ambient conditions; the solid background signal at 1.1 GPa, $I^{bkgd}_{solid}(Q)$; the corrected solid-background spectra, $I^{bkgd}(Q)$, given in Eq. (A1); and a subsequently obtained empty-cell-background spectra, $I^{bkgd}_{empty}(Q)$. Note the strong similarity between the corrected solid-background spectra and the empty-cell-background spectra. This agreement *cannot* be obtained without explicitly considering the TDS of the sample.

One final caution should be mentioned at this point: the

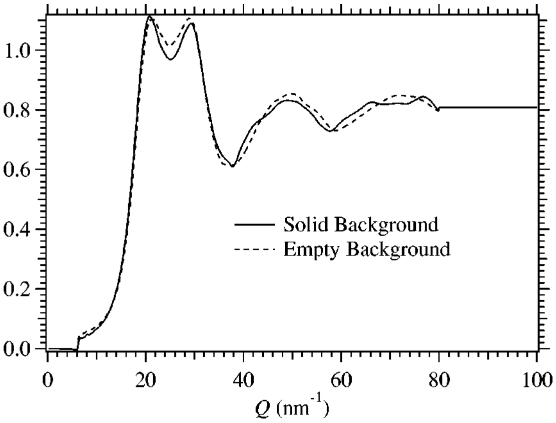

FIG. 14. Structure factors of ambient condition H_2O calculated using the empty-cell and corrected-solid background spectra with Q_{max}=80 nm^{-1}. The structure factors are very similar which is only the case when the solid background is very carefully corrected as described in this appendix.

isotropic form of the TDS used in Eqs. (32) and (A1) is really only appropriate in the case of a powder sample with many diffraction peaks distributed in Q so that the anisotropy in the TDS is effectively averaged out.[15] Our approach must be used with extreme caution if the solid is nearly a single crystal or if there are few diffraction peaks in the vicinity, as is always true at low Q. We found that very careful peak fitting was necessary to subtract the TDS sidebands near the first Bragg peaks in the region of Q near the dominant liquid peak. Fortunately, the TDS intensity is weak at small Q and careful attention the peak subtraction was sufficient to obtain the results shown in Figs. 13 and 14.

---

[1] Y. Katayama, T. Mizutani, W. Utsumi, O. Shimomura, M. Yamakata, and K. Funakoshi, Nature (London) **403**, 170 (2000).

[2] C. Sanloup, F. Guyot, P. Gillet, G. Fiquet, R. J. Hemley, M. Mezouar, and I. Martinez, Europhys. Lett. **52**, 151 (2000).

[3] J. Y. Raty, J. P. Gaspard, T. Le Bihan, M. Mezouar, and M. Bionducci, J. Phys.: Condens. Matter **11**, 10243 (1999).

[4] M. Mezouar, S. Bauchau, G. Blattmann, P. Faure, N. Rambert, and B. Sitaud (unpublished).

[5] M. B. Kruger and C. Meade, Phys. Rev. B **55**, 1 (1997).

[6] C. Meade, R. J. Hemley, and H. K. Mao, Phys. Rev. Lett. **69**, 1387 (1992).

[7] W. A. Crichton, M. Mezouar, T. Grande, S. Stølen, and A. Grzechnik, Nature (London) **414**, 622 (2001).

[8] R. LeToullec, J. P. Pinceaux, and P. Loubeyre, High Press. Res. **1**, 77 (1988).

[9] F. Datchi, R. Letoullec, and P. Loubeyre, J. Appl. Phys. **81**, 3333 (1997).

[10] J. H. Eggert, G. Weck, and P. Loubeyre (unpublished).

[11] M. Thoms, S. Bauchau, M. Kunz, T. Le Bihan, M. Mezouar, D. Häusermann, and D. Strawbridge, Nucl. Instrum. Methods Phys. Res. A **413**, 175 (1998).

[12] X-ray Research GmbH, www.marresearch.com, Norderstedt, Germany.

[13] A. Hammersley (unpublished).

[14] A. Hammersley, O. Svensson, M. Hanfland, A. Fitch, and D. Häusermann, High Press. Res. **14**, 235 (1996).

[15] B. E. Warren, *X-Ray Diffraction* (Addison-Wesley, Reading, MA, 1969).

[16] P. Debye, Ann. Phys. (Leipzig) **46**, 809 (1915).

[17] F. Hajdu, Acta Crystallogr., Sect. A: Cryst. Phys., Diffr., Theor. Gen. Crystallogr. **A28**, 250 (1972).

[18] J. M. Sorenson, G. Hura, R. M. Glaeser, and T. Head-Gordon, J. Chem. Phys. **113**, 9149 (2000).

[19] As as long as the x-ray energy is much less than the electron rest mass, the Klein-Nishina equation for the polarization dependence of incoherent Compton scattering reduces to Eq. (30) for the polarization dependence of coherent scattering. Thus, the polarization correction can be applied to the coherent and incoherent scattering simultaneously.

[20] C. H. Reinsch, Numer. Math. **10**, 177 (1967). As implemented in the program IGOR PRO by WaveMetrics, www.wavemetrics.com.

[21] J. Krogh-Moe, Acta Crystallogr. **9**, 951 (1956).

[22] N. Norman, Acta Crystallogr. **10**, 370 (1957).

[23] R. Kaplow, S. L. Strong, and B. L. Averbach, Phys. Rev. **138**, A1336 (1965).

[24] O. Gereben and L. Pusztai, Phys. Rev. B **50**, 14 136 (1994).

[25] O. Gereben and L. Pusztai, Phys. Chem. Liq. **31**, 159 (1996).

[26] Our sample was confined in the DAC with no applied force and a measured pressure of 0 ± 0.05 GPa. However, it is highly likely that some small pressure remained.

[27] D. H. Liebenberg, R. L. Mills, and J. C. Bronson, J. Appl. Phys. **45**, 741 (1974).

[28] A. Saul and W. Wagner, J. Phys. Chem. Ref. Data **18**, 1537 (1989).

[29] R. A. Aziz, J. Chem. Phys. **99**, 4518 (1993).

[30] G. Hura, J. M. Sorenson, R. M. Glaeser, and T. Head-Gordon, J. Chem. Phys. **113**, 9140 (2000).

[31] A. K. Soper, F. Bruni, and M. A. Ricci, J. Chem. Phys. **106**, 247 (1997).

[32] E. Schwegler, G. Galli, and F. Gygi, Phys. Rev. Lett. **84**, 2429 (2000).

[33] A. V. Okhulkov, Y. N. Demianets, and Y. E. Gorbaty, J. Chem. Phys. **100**, 1578 (1994).

[34] R. L. McGreevy and L. Pusztai, Mol. Simul. **1**, 359 (1988).